

Entropy production rate and correlations in a cavity magnomechanical system

Collins O. Edet^{1,2}, Muhammad Asjad^{3,*}, Denys Dutykh^{3,4}, Norshamsuri Ali⁵, and Obinna Abah^{6,†}

¹*Institute of Engineering Mathematics, Universiti Malaysia Perlis, 02600 Arau, Perlis, Malaysia*

²*Department of Physics, University of Cross River State, Calabar, Nigeria*

³*Department of Mathematics, Khalifa University, Abu Dhabi 127788, United Arab Emirates*

⁴*Causal Dynamics Pty Ltd, Perth, Australia*

⁵*Advanced Communication Engineering (ACE) Centre of Excellence, Universiti Malaysia Perlis, 01000 Kangar, Perlis, Malaysia*

⁶*School of Mathematics, Statistics and Physics, Newcastle University, Newcastle upon Tyne NE1 7RU, United Kingdom*



(Received 30 January 2024; revised 25 April 2024; accepted 16 May 2024; published 8 July 2024)

We present the irreversibility generated by a stationary cavity magnomechanical system composed of a yttrium iron garnet (YIG) sphere with a diameter of a few hundred micrometers inside a microwave cavity. In this system, the magnons, i.e., collective spin excitations in the sphere, are coupled to the cavity photon mode via magnetic dipole interaction and to the phonon mode via magnetostrictive force (optomechanical-like). We employ the quantum phase-space formulation of the entropy change to evaluate the steady-state entropy production rate and associated quantum correlation in the system. We find that the behavior of the entropy flow between the cavity photon mode and the phonon mode is determined by the magnon-photon coupling and the cavity photon dissipation rate. Interestingly, the entropy production rate can increase/decrease depending on the strength of the magnon-photon coupling and the detuning parameters. We further show that the amount of correlations between the magnon and phonon modes is linked to the irreversibility generated in the system for small magnon-photon coupling. Our results demonstrate the possibility of exploring irreversibility in driven magnon-based hybrid quantum systems and open a promising route for quantum thermal applications.

DOI: [10.1103/PhysRevResearch.6.033037](https://doi.org/10.1103/PhysRevResearch.6.033037)

I. INTRODUCTION

Hybrid quantum systems play a crucial role in the advancement of quantum technologies [1–6]. In the last decade, remarkable progress has been made in this field with applications spanning through quantum computing [5,7], quantum simulation [8], quantum communication [6], quantum sensing [9], and quantum thermodynamics [10]. A typical example is the cavity optomechanical system, which combines mechanical degrees of freedom with electromagnetic (EM) cavities [11]. Recently, hybrid quantum systems based on magnons, quanta of collective spin excitations in ordered ferrimagnetic materials, e.g., yttrium iron garnet (YIG), have attracted considerable attention due to great frequency tunability and very good coherence [4]. Magnons can be coherently coupled to different degrees of freedom, such as phonons via the magnetostrictive force [12], microwave photons via the magnetic dipole interaction [4,13,14], optical photons [15,16] and superconducting qubits [17–19]. The realization of this cavity magnomechanical system, a system of photon-magnon-phonon interaction with YIG spheres interacting with microwave cavities has open up possible

applications in the preparation of macroscopic quantum states [20], generation of squeezed states [21], the generation of high-performance detectors [22], entanglement generation [23,24], ground-state cooling [25], and quantum information processing [26–29].

Quantum technological and nanofabrication advancements have motivated the design of microscopic and coherent thermodynamic machines—quantum thermal machines [10]—as well as investigating the interplay between quantum information and thermodynamic processes [30]. Optomechanical thermal machines have been proposed in different configurations [31–37]. The irreversibility (such as, friction, disorder) that influences the machine thermodynamic processes/performance can be quantified by entropy production [38,39]. Thus, quantifying the degree of irreversible entropy generated in a dynamic process is useful for the distinctive description of the nonequilibrium processes, and decreasing it, enhances a thermal machine efficiency [40]. Based on quantum phase-space method, the measure of quantifying the irreversible entropy production of quantum systems that interact with nonequilibrium reservoirs has been formulated in Refs. [41–43] and experimentally verified in two distinct setup, an optomechanical system and a driven Bose-Einstein condensate coupled to a high-finesse cavity [44]. The effect of self-correlation on irreversible entropy production rate in a parametrically driven dissipative system has been investigated [45]. It has been recently shown that the presence of nonlinearity via an optical parametric oscillator placed inside the cavity optomechanical system influences the stationary state entropy production rate [46]. Moreover, it has been established that the entropy

*asjad_qau@yahoo.com

†obinna.abah@newcastle.ac.uk

Published by the American Physical Society under the terms of the [Creative Commons Attribution 4.0 International](https://creativecommons.org/licenses/by/4.0/) license. Further distribution of this work must maintain attribution to the author(s) and the published article's title, journal citation, and DOI.

produced in a bipartite quantum system is related to the amount of correlations shared by its subsystems [41].

Here, we investigate the generation of irreversibility in a hybrid cavity magnomechanical setup comprising a microwave cavity and a YIG sphere. In this system, magnons are simultaneously coupled to the phonons of the vibrational sphere via magnetostrictive interaction and to the cavity photons via magnetic-dipole interaction, while there is no direct interaction between the cavity mode and the mechanical mode. We find that the magnon-photon coupling and cavity photon dissipation rate influence the entropy production rate. Furthermore, we demonstrate that the amount of correlations in the cavity magnomechanical system deviates from the steady-state entropy production rate for large magnon-photon coupling.

The rest of this paper is organized as follows. In Sec. II, we present the physical model of the cavity magnomechanical system. We derive the linearized Hamiltonian of the system via quantum Langevin equations of motion and standard linearization techniques. In Sec. III, the stationary entropy production rate and quantum correlation quantified by mutual information are presented using the experimentally feasible parameters. Finally, the conclusions are summarized in Sec. IV.

II. CAVITY MAGNOMECHANICAL MODEL

We consider a hybrid cavity magnomechanical system, which consists of a microwave cavity and a small sphere (a one mm -diameter, highly polished YIG sphere is considered in Ref. [47,48]). The YIG sphere is positioned inside a three-dimensional microwave cavity. The YIG sphere is positioned close to the maximal microwave magnetic field of the cavity TE_{011} mode, and a variable external magnetic field H in the z axis is added to establish the magnon-photon coupling [47,49]. The coupling rate can be tailored by adjusting the position of the sphere. The magnons couple to phonons via the magnetostrictive effect. The vibrational modes (phonons) result from the geometric deformation of the YIG sphere because the magnon excitation inside the YIG sphere induces a varying magnetization. The magnomechanical coupling can be enhanced by directly driving the magnon mode with a microwave source [12]. In addition, the size of the sphere considered is much smaller than the wavelength of the microwave field, such that the interaction between cavity microwave photons and phonons can be neglected (i.e., the radiation pressure effect is negligible). Thus, the system has three modes: cavity photon, magnon, and phonon modes, which can be schematically depicted by the equivalent coupled harmonic oscillators model as shown in Fig. 1.

The Hamiltonian of the hybrid quantum system under rotating-wave approximation in a frame rotating with the frequency ω_d of the driving field can be expressed as ($\hbar=1$) [23,48]:

$$\hat{H} := \Delta_a \hat{a}^\dagger \hat{a} + \Omega_b \hat{b}^\dagger \hat{b} + \Delta_m \hat{m}^\dagger \hat{m} + g_{am} (\hat{a} \hat{m}^\dagger + \hat{a}^\dagger \hat{m}) + g_{mb} \hat{m}^\dagger \hat{m} (\hat{b} + \hat{b}^\dagger) + i(\Omega_d \hat{m}^\dagger - \Omega_d^* \hat{m}), \quad (1)$$

where the bosonic annihilation (creation) operators \hat{a} (\hat{a}^\dagger), \hat{b} (\hat{b}^\dagger) and \hat{m} (\hat{m}^\dagger) denote, respectively, cavity photon, phonon

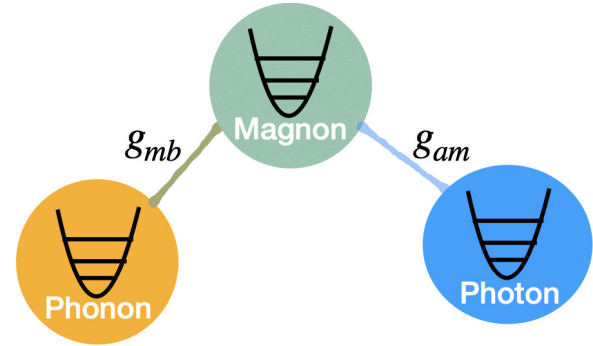


FIG. 1. Diagrammatic representation of a cavity magnomechanical system consisting of photon, magnon, and phonon modes. The magnon-photon interaction strength and the magnon-phonon interaction of coupling strength are denoted by g_{am} and g_{mb} , respectively.

and magnon modes whose resonant frequencies are taken to be ω_a , Ω_b , and ω_m correspondingly. The detuning parameters $\Delta_a := \omega_a - \omega_d$, where $\omega_a/2\pi = 10$ GHz [12], and $\Delta_m := \omega_m - \omega_d$. The uniform magnon mode frequency in the YIG sphere is $\omega_m = \gamma_g H$, where $\gamma_g/2\pi = 28$ GHz/T is the gyromagnetic ratio, and we set ω_m at the Kittel mode frequency [50], which can lead to cavity polaritons by strongly coupling magnon and cavity photons. The parameters g_{am} and g_{mb} are the optomagnon (photon-magnon) and magnomechanical (magnon-phonon) interaction coupling strengths, respectively. The last term, $(\Omega_d \hat{m}^\dagger - \Omega_d^* \hat{m})$ in the Hamiltonian describes the external driving of the magnon mode. The Rabi frequency $\Omega_d \equiv \frac{\sqrt{5}}{4} \gamma_g \sqrt{N_t} B_0$ (assuming low-lying excitations) denotes the coupling strength of the drive magnetic field [23]. The amplitude and frequency of the drive field are B_0 and ω_d , respectively, and the total number of spins $N_t = \rho V$, where V is the volume of the sphere and $\rho = 4.22 \times 10^{27} \text{ m}^{-3}$ is the spin density of the YIG sphere. Each of the modes is coupled to an independent noise reservoir, their energy decay rates are γ_a , γ_m , and γ_b , for photon, magnon, and phonon respectively. Experimentally, g_{mb} is extremely weak [12], but the magnomechanical interaction can be enhanced by driving the magnon mode with a strong microwave field [47,49]. The magnon-photon coupling rate g_{am} can be larger than the dissipation rates of the cavity and magnon modes, γ_a and γ_m , entering into the strong coupling regime, $g_{am} > (\gamma_a + \gamma_m)/2$ [13,14].

As a result of strong driving, the Hamiltonian in Eq. (1) can be linearized around the coherent steady-state amplitude: $\hat{\mathcal{O}} \rightarrow \mathcal{O}_s + \hat{\mathcal{O}}$ ($\mathcal{O} \in \{a, b, m\}$), where \mathcal{O}_s and the operators $\hat{\mathcal{O}}$, represent the steady-state amplitudes and quantum fluctuations of the corresponding mode. The steady-state amplitudes can be defined as

$$m_s = \frac{\Omega_d (i\Delta_a + \gamma_a)}{g_{am}^2 + (i\Delta_m + \gamma_m)(i\Delta_a + \gamma_a)}, \quad (2)$$

and $b_s = -i g_{mb} |m_s|^2 / (i\Omega_b + \gamma_b)$. Then, the linearized Hamiltonian can be derived as

$$\hat{H}_{lin} = \Delta_a \hat{a}^\dagger \hat{a} + \Omega_b \hat{b}^\dagger \hat{b} + \tilde{\Delta}_m \hat{m}^\dagger \hat{m} + g_{am} (\hat{a} \hat{m}^\dagger + \hat{a}^\dagger \hat{m}) + (\mathcal{G}_{mb}^* \hat{m} + \mathcal{G}_{mb} \hat{m}^\dagger) (\hat{b} + \hat{b}^\dagger), \quad (3)$$

where the enhanced magnon-phonon coupling $\mathcal{G}_{mb} = g_{mb}m_s$, and $\tilde{\Delta}_m = \Delta_m - g_{mb}(b_s + b_s^*)$ is the effective magnon detuning incorporating the magnetostriction. For the considered parameters, $g_{mb}(b_s + b_s^*) \ll \Delta_m$, so we can have, $\tilde{\Delta}_m \approx \Delta_m$. Since the driving field affects m_s , we can improve \mathcal{G}_{mb} by adjusting the external driving field Ω_d .

From the Hamiltonian in Eq. (3), we obtain the quantum Langevin equations as;

$$\begin{aligned}\dot{\hat{a}} &= -(i\Delta_a + \gamma_a)\hat{a} - ig_{am}\hat{m} + \sqrt{2\gamma_a}\hat{a}_{in}, \\ \dot{\hat{m}} &= -(i\tilde{\Delta}_m + \gamma_m)\hat{m} - ig_{am}\hat{a} - i\mathcal{G}_{mb}(\hat{b} + \hat{b}^\dagger) + \sqrt{2\gamma_m}\hat{m}_{in}, \\ \dot{\hat{b}} &= -(i\Omega_b + \gamma_b)\hat{b} - i(\mathcal{G}_{mb}\hat{m}^\dagger + \mathcal{G}_{mb}^*\hat{m}) + \sqrt{2\gamma_b}\hat{b}_{in},\end{aligned}\quad (4)$$

where $\hat{f}_{in} \in \{\hat{a}_{in}, \hat{m}_{in}, \hat{b}_{in}\}$ are input noise operators for the cavity, magnon, and mechanical modes, respectively, which are zero mean and characterized by the following correlation functions [51]: $\langle \hat{f}_{in}(t)\hat{f}_{in}^\dagger(t') \rangle = (\mathcal{N}_k + 1)\delta(t - t')$ and $\langle \hat{f}_{in}^\dagger(t)\hat{f}_{in}(t') \rangle = \mathcal{N}_k\delta(t - t')$, where $\mathcal{N}_k = 1/(e^{\hbar\omega_k/k_B T} - 1)$ ($k \in \{a, m\}$), are the equilibrium mean thermal photon and magnon number, respectively, while $\mathcal{N}_b = 1/(e^{\hbar\Omega_b/k_B T} - 1)$ is the equilibrium mean thermal phonon number, T is the environmental temperature, and k_B is the Boltzmann constant. Equation (4) represents the evolution of the fluctuation incorporating the interplay with the environment via the noise operators [25].

Since the nature of the noise is Gaussian, all the information is contained in the first- and second-order moments of the operators. In particular, it is convenient to introduce the quadratures \hat{x} and \hat{y} of the photon, magnon, and phonon modes by using the relation $\hat{\mathcal{O}} = (\hat{x}_{\mathcal{O}} + i\hat{y}_{\mathcal{O}})/\sqrt{2}$ with $\mathcal{O} \in \{a, m, b\}$, and elements of the corresponding covariance matrix are defined as $\mathcal{V}_{ij} = \frac{1}{2}\langle \mathcal{R}_i(\infty)\mathcal{R}_j(\infty) + \mathcal{R}_j(\infty)\mathcal{R}_i(\infty) \rangle$, ($i, j \in \{1, 2, 3, 4, 5, 6\}$). Here, $\mathcal{R}_i(t) := [\hat{x}_a, \hat{y}_a, \hat{x}_m, \hat{y}_m, \hat{x}_b, \hat{y}_b]^\top$ is the column vector of quadratures and the stationary covariance matrix is obtained by solving the algebraic equation $\mathcal{A}^\top \mathcal{V} + \mathcal{A} \mathcal{V} + \mathcal{D} = 0$, where $\mathcal{D} = \text{diag}(\mathcal{D}_a, \mathcal{D}_a, \mathcal{D}_m, \mathcal{D}_m, \mathcal{D}_b, \mathcal{D}_b)$ with $\mathcal{D}_i = \gamma_i(2\mathcal{N}_i + 1)$ with $i \in \{a, m, b\}$ and the drift matrix \mathcal{A} is expressed as:

$$\mathcal{A} = \begin{pmatrix} -\gamma_a & \Delta_a & 0 & g_{am} & 0 & 0 \\ -\Delta_a & -\gamma_a & -g_{am} & 0 & 0 & 0 \\ 0 & g_{am} & -\gamma_m & \tilde{\Delta}_m & -\mathcal{G}_{mb} & 0 \\ -g_{am} & 0 & -\tilde{\Delta}_m & -\gamma_m & 0 & 0 \\ 0 & 0 & 0 & 0 & 0 & \Omega_b \\ 0 & 0 & 0 & \mathcal{G}_{mb} & -\Omega_b & -\gamma_b \end{pmatrix}. \quad (5)$$

The system must be stable for a steady state to exist; to ascertain this, the Routh-Hurwitz criterion [52] is employed to characterize the stability of the system. To achieve this, the real part of the spectrum of the drift matrix \mathcal{A} , Eq. (5), must be negative, this means that all the eigenvalues of the drift matrix \mathcal{A} have nonpositive real parts.

III. ENTROPY PRODUCTION RATE

The basic thermodynamics principle asserts the entropy of an open system, (classical or quantum) evolves as:

$$\frac{dS}{dt} = \Pi - \Phi, \quad (6)$$

where $\Pi \geq 0$ is the irreversible entropy production rate and Φ is the entropy flow from the system to the reservoir. In thermal equilibrium, the steady states are characterized by $dS/dt = \Pi = \Phi = 0$. However, when the system is connected to multiple reservoirs or being externally driven, it may instead reach a nonequilibrium steady state where $dS/dt = 0$ but $\Pi = \Phi \geq 0$. In this nonequilibrium steady-state case, the system is characterized by the continuous production of entropy, all of which flows to the reservoir.

We now move to study the entropy production rate from a multipartite system. In analogy with the bipartite case [41], we combine quantum phase-space methods and the Fokker-Planck equation to characterize the irreversible entropy production of quantum systems interacting with reservoirs. In general, the entropy production rate of the quantum system described in Sec. II is given by (see Appendix):

$$\Pi_s := \sum_{i=1}^3 2\gamma_i \left(\frac{\mathcal{V}_{2i-1, 2i-1} + \mathcal{V}_{2i, 2i}}{2\mathcal{N}_i + 1} - 1 \right), \quad (7)$$

where $\Gamma_i \in \{\Gamma_a, \Gamma_m, \Gamma_b\}$ with $\Gamma \in \{\gamma, \mathcal{N}\}$.

Here, we focus on characterizing the entropy production rates in a cavity magnomechanical system. Without loss of generality, we consider the effective entropy flow between the magnon mode and the mechanical resonator. Thus, the rate of entropy production Π_s at a steady state reads

$$\Pi_s = 2\gamma_m \left(\frac{\mathcal{V}_{33} + \mathcal{V}_{44}}{2\mathcal{N}_m + 1} - 1 \right) + 2\gamma_b \left(\frac{\mathcal{V}_{55} + \mathcal{V}_{66}}{2\mathcal{N}_b + 1} - 1 \right). \quad (8)$$

We remark, when the system is in the equilibrium state, we have $\mathcal{V}_{33} + \mathcal{V}_{44} = 2\mathcal{N}_m + 1$, $\mathcal{V}_{55} + \mathcal{V}_{66} = 2\mathcal{N}_b + 1$, and hence, $\Pi_s \equiv 0$.

To proceed, we study the entropy production rate in a magnon-phonon-photon system at a steady state in the resolved sideband, where the magnon dissipation rate is comparable to or well below the mechanical resonance frequency (i.e., $\gamma_m < \Omega_b$). We assume the following parameters close to those employed in the experimental realizations [12], as the phonon frequency $\Omega_b/2\pi = 10$ MHz, the cavity dissipation rate $\gamma_a/2\pi = 3$ MHz, the magnon dissipation rate $\gamma_m/2\pi = 1$ MHz, the phonon damping rate $\gamma_b = 300$ Hz, the phonon-magnon coupling $g_{mb}/2\pi \simeq 1$ Hz, and the temperature $T = 20$ – 100 mK (i.e., $\mathcal{N}_b \sim 200$) and the thermal magnon occupation number $\mathcal{N}_m \sim 10^{-9}$ to $\mathcal{N}_m \sim 10^{-2}$ for magnon frequency $\omega_m = 8.5$ GHz [53]. Hence, the discussions about the entropy production and correlation is experimentally feasible. In the following analysis, we will utilize dimensionless quantities; that is, the quantities will be expressed in units of the phonon frequency, Ω_b . In Fig. 2, we present the entropy production rate Π_s is plotted as a function of the normalized magnon detuning Δ_m/Ω_b for various values of the photon-magnon coupling g_{am} . In Fig. 2(a) and 2(b), we consider the dissipation rate of the cavity $\gamma_a = 10^{-1}\Omega_b$ for distinct occupation number $\mathcal{N}_b = 10$ and $\mathcal{N}_b = 100$, respectively. It

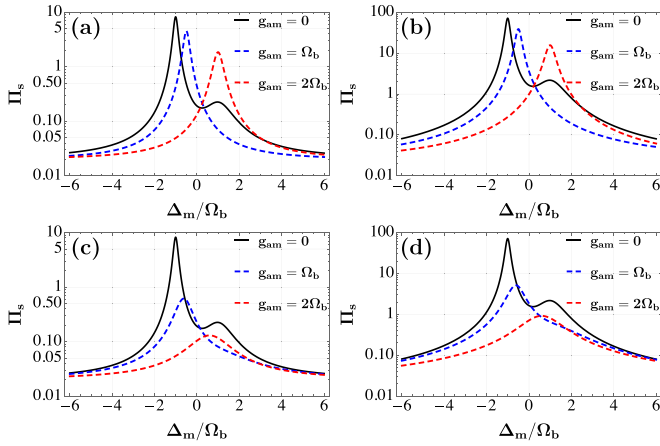


FIG. 2. Plot of entropy Π_s (blue dashed) as a function of normalized magnon detuning Δ_m/Ω_b for different values of magnon-photon coupling $g_{am} = 0$ (black curve), $g_{am} = \Omega_b$ (blue curve) and $g_{am} = 2\Omega_b$ (red curve), where (a) $\mathcal{N}_b = 10$, (b) $\mathcal{N}_b = 100$, (c), $\mathcal{N}_b = 10$, and (d) $\mathcal{N}_b = 100$. In (a) and (b) $\gamma_a = 0.1\Omega_b$, and $\gamma_a = \Omega_b$ in (c) and (d). The other parameters are $\mathcal{G}_{mb} = 10^{-1}\Omega_b$, $\gamma_b = 10^{-2}\Omega_b$, and $\gamma_m = \Omega_b/2$.

can be seen that in the absence of magnon-photon interaction $g_{am} = 0$, the entropy production rate Π_s peaks at $\Delta_m/\Omega_b = \pm 1$. The two peaks in the rate of entropy production for positive/negative detuning imply the cooling/heating processes behave differently in two distinct regimes of the system. For nonzero g_{am} , the smaller peak smears out with reduced maximum Π_s . We observe that for $g_{am} = \Omega_b$ ($g_{am} = 2\Omega_b$), the maximum Π_s is in the red (blue) sideband region. The maximum entropy flow between the phonon mode and the effective magnon mode occurs when $g_{am} = 2\Omega_b$, at $\Delta_m = \omega_b$. Figures 2(c) and 2(d) show more clearly the effect and interplay between the cavity photon dissipation rate and the magnon-photon coupling. For the case of $\gamma_b = \Omega_b$, Fig. 2(c) and 2(d), the value of Π_s further decreases with a broaden peak as magnon-photon coupling g_{am} increases. In the blue sideband, for $g_{am} \neq 0$, the value of Π_s is always reduced compare to the $g_{am} = 0$ scenario. It can be seen that Π_s could be enhanced close to the negative detuning region $\Delta_m < 0$. The effects of thermal fluctuations of the environment on the entropy production rate is shown in Fig. 2. Figure 2 shows that increasing the phonon thermal excitation (occupation number) \mathcal{N}_b , increases Π_s in magnitude [see the magnitude of Π_s in Figs. 2(a) and 2(c) compare to Figs. 2(b) and 2(d), respectively]. The nonuniform behavior when varying g_{am} for different γ_a is a direct implication of the complex nature of the interaction between the dissipation processes in the cavity magnomechanical system.

In Fig. 3, the effects of the cavity photon dissipation rate of the environment on the entropy production rate is explored. We present in Fig. 3(a), the plot of the entropy production rate as a function of magnon-photon coupling with various values of the cavity decay rate, while Fig. 3(b) shows the entropy production rate as function of cavity decay rate with different values of the magnon-photon coupling. For large thermal excitations, $\mathcal{N}_b = 100$, and $\Delta_m = \Omega_b$, the entropy production rates decrease in oscillatory form as

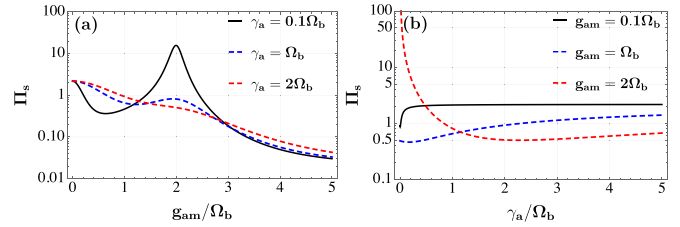


FIG. 3. (a) The entropy production rate Π_s as a function of magnon-photon coupling g_{am}/Ω_b for different values of cavity photon decay rate $\gamma_a = 10^{-1}\Omega_b$ (black curve), $\gamma_a = \Omega_b$ (blue curve), and $\gamma_a = 2\Omega_b$ (red curve). (b) Entropy production rate Π_s as a function of cavity photon decay rate γ_a/Ω_b for different values of magnon-photon coupling $g_{am} = 10^{-1}\Omega_b$ (black curve), $g_{am} = \Omega_b$ (blue curve), and $g_{am} = 2\Omega_b$ (red curve). Other parameters are $\mathcal{N}_b = 100$, $\Delta_m = \Omega_b$, $\mathcal{G}_{mb} = 10^{-1}\Omega_b$, $\gamma_b = 10^{-2}\Omega_b$, and $\gamma_m = \Omega_b/2$.

the magnon-photon coupling increases. For $\gamma_a = 10^{-1}\Omega_b$, the maximum entropy production rate corresponds to the $g_{am} = 2\Omega_b$. It can be seen that the entropy production rate can be increase/decrease by tuning the cavity decay value γ_a and the magnon-photon coupling, see $g_{am} \simeq 0.2-3\Omega_b$. The entropy production rate Π_s linearly decreases with respect to the magnon-photon coupling when $g_{am} > 3/\Omega_b$ but the value slightly increase when we increase γ_a . This nonmonotonic behavior (increase/decrease) of the entropy production with respect to the magnon-photon coupling can be attributed to the imbalance in populations between the interacting modes induced by the environment. Furthermore, Fig. 3(b) shows that the entropy production rate can increase/decrease when $\gamma_a < g_{am}$ but increases slightly after $\gamma_a = g_{am}$. In the region, $\gamma_a \gg g_{am}$, the entropy production rate saturates to a quasiconstant value with decreasing value as the magnon-photon g_{am} increases. This is due to the fact that the individual modes are far from resonance and they are effectively decoupled, in such a way that the individually thermalize their own bath. Next, we analyze the behavior of the entropy production rate with respect to the amount of correlations shared between the magnon and phonon modes. For coupled quantum system, it has been demonstrated that the irreversibility generated by the dissipative system at steady state and the total amount of correlations shared between the subsystems are closely related in small coupling limit as [41]; $\mathcal{I} \approx \Pi_s / (2\gamma_{tot})$, where \mathcal{I} is the quantum mutual information between the modes at the stationary state and γ_{tot} is the sum of the dissipation rates to the local baths. Since the quantum noises are Gaussian, the mutual information between the magnon and phonon modes can be computed as [54]:

$$\mathcal{I}(\mathcal{V}_{a;b}) = \frac{1}{2} \ln \left(\frac{\det(\mathcal{V}_m) \det(\mathcal{V}_b)}{\det(\mathcal{V}_{mb})} \right), \quad (9)$$

where \mathcal{V}_m (\mathcal{V}_b) is the covariance matrix of magnon (mechanical) mode and \mathcal{V}_{ab} describes the correlation between the magnon and the phonon modes.

In Fig. 4, we show a comparative plot of the entropy production rate Π_s to the correlations established by the cavity magnomechanical system, as quantified by the mutual information \mathcal{I} . Considering small thermal phonon excitation, $\mathcal{N}_b = 10$, Fig. 4(a) shows a good similarity in both Π_s and \mathcal{I} curves

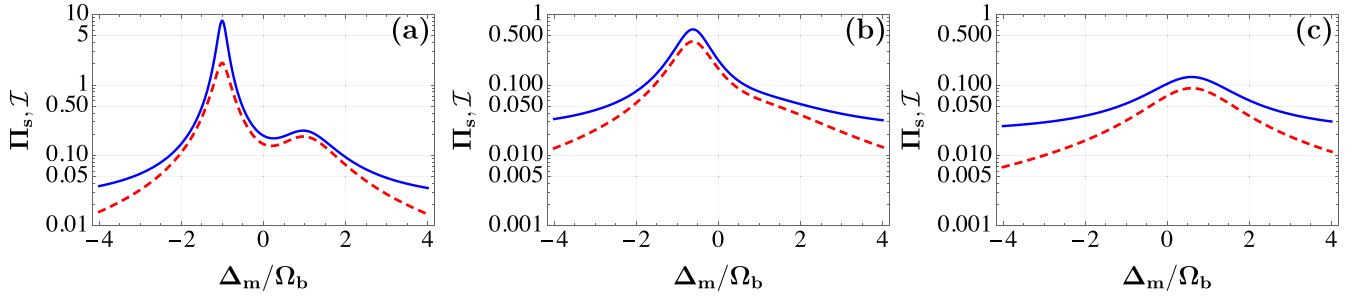


FIG. 4. Entropy rate Π_s (blue curve) and mutual information \mathcal{I} (red curve) as a function of normalized magnon detuning Δ_m/Ω_b for different values of magnon-photon coupling (a) $g_{am} = 0$, (b) $g_{am} = \Omega_b$, and (c) $g_{am} = 2\Omega_b$. Here, other parameters are $\gamma_a = \Omega_b$, $\mathcal{N}_b = 10$, $\mathcal{G}_{mb} = 10^{-1}\Omega_b$, $\gamma_b = 10^{-2}\Omega_b$, and $\gamma_m = \Omega_b/2$.

for $|\Delta_m/\Omega_b| \leq 2$. As the magnon-photon coupling increases, both the entropy production rate and mutual information are decreasing as well as an increase in both quantities deviation, see Figs. 4(b) and 4(c). The increase in deviation between Π_s and \mathcal{I} for increasing detuning Δ_m , clearly demonstrates the interplay among magnon-photon coupling and dissipation rates. This shows that degree of irreversibility induced by the stationary process is directly related to the amount of correlations shared in the system.

IV. CONCLUSIONS

We have investigated the entropy production rate in a hybrid magnomechanical system where a microwave cavity mode is coupled to a magnon mode in a YIG sphere, and the latter is simultaneously coupled to a phonon mode via magnetostrictive force. Specifically, within the quantum phase-space formulation of the entropy change, we evaluate the steady-state entropy production rate and associated quantum correlation in the hybrid system. We have shown that the entropy flow between the effective magnon mode and the phonon mode is influenced by the magnon-photon coupling and the cavity photon dissipation rate. Our numerical analysis shows nonuniform behavior of irreversibility resulting from the complex and competing nature of the interactions in the cavity magnomechanical system. We find that the entropy production rate can be increased/decreased when the cavity decay rate is less than the magnon-photon coupling. Furthermore, we studied the range of validity of the link between irreversibility and the amount of correlations in a mesoscopic quantum system. These results provide insight into the impact of magnonics on the thermodynamics processes of hybrid quantum systems. Finally, we anticipate that our study will open new perspectives for quantum thermodynamics applications, such as realizing thermal machines in the deep quantum regime and quantum thermal transport.

ACKNOWLEDGMENTS

C.O.E. and N.A. have been supported by LRGS Grant LRGS/1/2020/UM/01/5/2 (9012-00009) provided by the Ministry of Higher Education of Malaysia (MOHE). M.A. and D.D. have been supported by the Khalifa University of Science and Technology under Award No. FSU- 2023-014.

APPENDIX: ENTROPY PRODUCTION

In this Appendix, we provide the explicit expression for the entropy production rate presented in Eq. (7). Considering the Gaussian nature of the quantum system, their states are characterized by the Wigner function of the form

$$\mathcal{W}(\mathcal{R}) = \frac{1}{\pi^n \sqrt{\det \mathcal{V}}} \exp\left(-\frac{1}{2} \mathcal{R}^\top \mathcal{V}^{-1} \mathcal{R}\right), \quad (\text{A1})$$

where n is the number of the bosonic mode, $\bar{\mathcal{R}} = \langle \mathcal{R} \rangle$, and \mathcal{V} is the covariance matrix (CM), whose entries are given by $\mathcal{V}_{ij} = \frac{1}{2} \langle \mathcal{R}_i \mathcal{R}_j + \mathcal{R}_j \mathcal{R}_i \rangle$. The entropy of the Gaussian system is associated to the corresponding Shannon entropy (Wigner entropy) of the Wigner distribution.

Following the quantum Langevin equations for the system dynamics described in Sec. II, we can recast the Fokker-Planck equation for the Wigner function $\mathcal{W}(u, t)$ as a local conservation equation

$$\partial_t \mathcal{W} = -\partial_u \mathcal{J}(u, t), \quad (\text{A2})$$

where $u = (x_a, y_a, x_m, y_m, x_b, y_b)^\top$ is a point in phase space, ∂_u is the phase-space gradient, and \mathcal{J} is the total probability current vector that reads

$$\mathcal{J}(u, t) = \mathcal{A} u \mathcal{W}(u, t) - \frac{1}{2} \mathcal{D} \partial_u \mathcal{W}(u, t). \quad (\text{A3})$$

For the three-mode bosonic system model that we consider, the drift matrix \mathcal{A} and the diffusion matrix \mathcal{D} are defined in Sec. II [Eq. (5)]. Then, introducing the time-reversal operator $E = \text{diag}(1, -1, 1, -1, 1, -1)$, the dynamical variables can be split according to their symmetry. The drift matrix \mathcal{A} can be rewritten by splitting it into the irreversible part \mathcal{A}^{irr} , which is even under time reversal and the reversible part \mathcal{A}^{rev} that is odd [41]. They can be evaluated as $\mathcal{A}^{\text{irr}} := \frac{1}{2}(\mathcal{A} + E \mathcal{A} E^\top)$ and $\mathcal{A}^{\text{rev}} := \frac{1}{2}(\mathcal{A} - E \mathcal{A} E^\top)$. The irreversible part is associated with the damping rates, while the reversible part comes from the Hamiltonian part of the dynamics. The drift matrix separation results in splitting of the probability currents as $\mathcal{J}(u, t) \equiv \mathcal{J}^{\text{rev}}(u, t) + \mathcal{J}^{\text{irr}}(u, t)$, where

$$\mathcal{J}^{\text{rev}}(u, t) := \mathcal{A}^{\text{rev}} u \mathcal{W}(u, t), \quad (\text{A4})$$

and

$$\mathcal{J}^{\text{irr}}(u, t) := \mathcal{A}^{\text{irr}} u \mathcal{W}(u, t) - \frac{1}{2} \mathcal{D} \partial_u \mathcal{W}(u, t). \quad (\text{A5})$$

Taking the derivative of the Wigner entropy with respect to time and integrating by parts, we get

$$S_W = \int d^2\alpha (\mathcal{J}^{\text{irr}} \mathcal{W})^\top \left(\frac{\partial_u \mathcal{W}}{\mathcal{W}} \right). \quad (\text{A6})$$

Equation (A6) can be rewritten in the usual form in terms of the entropy production rate [41]:

$$\Pi = \frac{1}{2} \int du \frac{1}{\mathcal{W}(u, t)} \mathcal{J}^{\text{irr}}(u, t)^\top D^{-1} \mathcal{J}^{\text{irr}}(u, t), \quad (\text{A7})$$

and entropy flux rate

$$\Phi = -\frac{1}{2} \int du \mathcal{J}^{\text{irr}}(u, t) D^{-1} A^{\text{irr}} u. \quad (\text{A8})$$

Moreover, for a Gaussian state, $\partial_u \mathcal{W}_\sigma(u, t) = -\mathcal{W}_\sigma(u, t) \mathcal{V}^{-1}(t) u$, then the irreversible component of probability current $\mathcal{J}^{\text{irr}}(u, t) = \mathcal{W}_\sigma(u, t) (\mathcal{A}^{\text{irr}} u + D) \mathcal{V}^{-1}(t) u$. Therefore, the explicit integration of Eq. (A7) gives the entropy production rate as [41]

$$\Pi = \frac{1}{2} \text{tr}[\mathcal{V}^{-1} \mathcal{D}] + 2 \text{tr}[\mathcal{A}^{\text{irr}}] + 2 \text{tr}[(\mathcal{A}^{\text{irr}})^\top \mathcal{D}^{-1} \mathcal{A}^{\text{irr}} \mathcal{V}]. \quad (\text{A9})$$

For the case of three-mode bosonic system, in stationary state, we obtain

$$\begin{aligned} \Pi_s &= 2\gamma_a \left(\frac{\mathcal{V}_{11} + \mathcal{V}_{22}}{2\mathcal{N}_a + 1} - 1 \right) + 2\gamma_m \left(\frac{\mathcal{V}_{33} + \mathcal{V}_{44}}{2\mathcal{N}_m + 1} - 1 \right) \\ &\quad + 2\gamma_b \left(\frac{\mathcal{V}_{55} + \mathcal{V}_{66}}{2\mathcal{N}_b + 1} - 1 \right) \end{aligned} \quad (\text{A10})$$

$$= \sum_{i=1}^3 2\gamma_i \left(\frac{\mathcal{V}_{2i-1, 2i-1} + \mathcal{V}_{2i, 2i}}{2\mathcal{N}_i + 1} - 1 \right), \quad (\text{A11})$$

where $\Gamma_i \in \{\Gamma_a, \Gamma_m, \Gamma_b\}$ with $\Gamma \in \{\gamma, \mathcal{N}\}$.

Within this framework, the rate of entropy production Π_s at steady state for two coupled oscillators mode is expressed as follows [41,44],

$$\begin{aligned} \Pi_s &= \text{Tr}(2\mathcal{A}^{\text{irr}} \mathcal{D}^{-1} \mathcal{A}^{\text{irr}} \mathcal{V} + \mathcal{A}^{\text{irr}}) \\ &= 2\gamma_m \left(\frac{\mathcal{V}_{33} + \mathcal{V}_{44}}{2\mathcal{N}_m + 1} - 1 \right) + 2\gamma_b \left(\frac{\mathcal{V}_{55} + \mathcal{V}_{66}}{2\mathcal{N}_b + 1} - 1 \right), \end{aligned} \quad (\text{A12})$$

where $\mathcal{A}^{\text{irr}} = \text{diag}\{0, 0, -\gamma_m, -\gamma_m, -\gamma_b, -\gamma_b\}$. This is the expression given in the main text.

-
- [1] Z.-L. Xiang, S. Ashhab, J. Q. You, and F. Nori, Hybrid quantum circuits: Superconducting circuits interacting with other quantum systems, *Rev. Mod. Phys.* **85**, 623 (2013).
- [2] B. Bauer, D. Wecker, A. J. Millis, M. B. Hastings, and M. Troyer, Hybrid quantum-classical approach to correlated materials, *Phys. Rev. X* **6**, 031045 (2016).
- [3] J. Li, X. Yang, X. Peng, and C.-P. Sun, Hybrid quantum-classical approach to quantum optimal control, *Phys. Rev. Lett.* **118**, 150503 (2017).
- [4] D. Lachance-Quirion, Y. Tabuchi, A. Gloppe, K. Usami, and Y. Nakamura, Hybrid quantum systems based on magnonics, *Appl. Phys. Express* **12**, 070101 (2019).
- [5] A. Clerk, K. Lehnert, P. Bertet, J. Petta, and Y. Nakamura, Hybrid quantum systems with circuit quantum electrodynamics, *Nature Phys.* **16**, 257 (2020).
- [6] A. Callison and N. Chancellor, Hybrid quantum-classical algorithms in the noisy intermediate-scale quantum era and beyond, *Phys. Rev. A* **106**, 010101 (2022).
- [7] A. C. Potter and R. Vasseur, Entanglement dynamics in hybrid quantum circuits, in *Entanglement in Spin Chains* (Springer, Berlin, 2022), pp. 211–249.
- [8] M. Wallquist, K. Hammerer, P. Rabl, M. Lukin, and P. Zoller, Hybrid quantum devices and quantum engineering, *Phys. Scr.* **T137**, 014001 (2009).
- [9] C. L. Degen, F. Reinhard, and P. Cappellaro, Quantum sensing, *Rev. Mod. Phys.* **89**, 035002 (2017).
- [10] N. M. Myers, O. Abah, and S. Deffner, Quantum thermodynamic devices: From theoretical proposals to experimental reality, *AVS Quantum Science* **4**, 027101 (2022).
- [11] M. Aspelmeyer, T. J. Kippenberg, and F. Marquardt, *Cavity Optomechanics: Nano- and Micromechanical Resonators Interacting with Light* (Springer, Berlin, 2014).
- [12] X. Zhang, C.-L. Zou, L. Jiang, and H. X. Tang, Cavity magnomechanics, *Sci. Adv.* **2**, e1501286 (2016).
- [13] Y. Tabuchi, S. Ishino, T. Ishikawa, R. Yamazaki, K. Usami, and Y. Nakamura, Hybridizing ferromagnetic magnons and microwave photons in the quantum limit, *Phys. Rev. Lett.* **113**, 083603 (2014).
- [14] L. Bai, M. Harder, Y. P. Chen, X. Fan, J. Q. Xiao, and C.-M. Hu, Spin pumping in electro-dynamically coupled magnon-photon systems, *Phys. Rev. Lett.* **114**, 227201 (2015).
- [15] A. Osada, A. Gloppe, R. Hisatomi, A. Noguchi, R. Yamazaki, M. Nomura, Y. Nakamura, and K. Usami, Brillouin light scattering by magnetic quasivortices in cavity optomagnonics, *Phys. Rev. Lett.* **120**, 133602 (2018).
- [16] J. A. Haigh, A. Nunnenkamp, A. J. Ramsay, and A. J. Ferguson, Triple-resonant Brillouin light scattering in magneto-optical cavities, *Phys. Rev. Lett.* **117**, 133602 (2016).
- [17] Y. Tabuchi, S. Ishino, A. Noguchi, T. Ishikawa, R. Yamazaki, K. Usami, and Y. Nakamura, Coherent coupling between a ferromagnetic magnon and a superconducting qubit, *Science* **349**, 405 (2015).
- [18] S. P. Wolski, D. Lachance-Quirion, Y. Tabuchi, S. Kono, A. Noguchi, K. Usami, and Y. Nakamura, Dissipation-based quantum sensing of magnons with a superconducting qubit, *Phys. Rev. Lett.* **125**, 117701 (2020).
- [19] Y. Li, V. G. Yefremenko, M. Lisovenko, C. Trevillian, T. Polakovic, T. W. Cecil, P. S. Barry, J. Pearson, R. Divan, V. Tyberkevych, C. L. Chang, U. Welp, W.-K. Kwok, and V. Novosad, Coherent coupling of two remote magnonic resonators mediated by superconducting circuits, *Phys. Rev. Lett.* **128**, 047701 (2022).
- [20] F.-X. Sun, S.-S. Zheng, Y. Xiao, Q. Gong, Q. He, and K. Xia, Remote generation of magnon Schrödinger cat state via magnon-photon entanglement, *Phys. Rev. Lett.* **127**, 087203 (2021).

- [21] S. Huang, L. Deng, and A. Chen, Squeezed states of magnons and phonons in a cavity magnomechanical system with a microwave parametric amplifier, *Ann. Phys. (Berlin)* **535**, 2300095 (2023).
- [22] C. A. Potts, E. Varga, V. A. Bittencourt, S. V. Kusminskiy, and J. P. Davis, Dynamical backaction magnomechanics, *Phys. Rev. X* **11**, 031053 (2021).
- [23] J. Li, S.-Y. Zhu, and G. S. Agarwal, Magnon-photon-phonon entanglement in cavity magnomechanics, *Phys. Rev. Lett.* **121**, 203601 (2018).
- [24] Z.-Q. Liu, Y. Liu, L. Tan, and W.-M. Liu, Reservoir engineering strong magnomechanical entanglement via dual-mode cooling, *Ann. Phys. (Berlin)* **535**, 2200660 (2023).
- [25] M. Asjad, J. Li, S.-Y. Zhu, and J. You, Magnon squeezing enhanced ground-state cooling in cavity magnomechanics, *Fund. Res.* **3**, 3 (2023).
- [26] H. Tan, Genuine photon-magnon-phonon Einstein-Podolsky-Rosen steerable nonlocality in a continuously-monitored cavity magnomechanical system, *Phys. Rev. Res.* **1**, 033161 (2019).
- [27] Y. Li, W. Zhang, V. Tyberkevych, W.-K. Kwok, A. Hoffmann, and V. Novosad, Hybrid magnonics: Physics, circuits, and applications for coherent information processing, *J. Appl. Phys.* **128**, 130902 (2020).
- [28] J. Li, Y.-P. Wang, W.-J. Wu, S.-Y. Zhu, and J.-Q. You, Quantum network with magnonic and mechanical nodes, *PRX Quantum* **2**, 040344 (2021).
- [29] H. Yuan, Y. Cao, A. Kamra, R. A. Duine, and P. Yan, Quantum magnonics: When magnon spintronics meets quantum information science, *Phys. Rep.* **965**, 1 (2022).
- [30] J. Goold, M. Huber, A. Riera, L. del Rio, and P. Skrzypczyk, The role of quantum information in thermodynamics—a topical review, *J. Phys. A: Math. Theor.* **49**, 143001 (2016).
- [31] K. Zhang, F. Bariani, and P. Meystre, Quantum optomechanical heat engine, *Phys. Rev. Lett.* **112**, 150602 (2014).
- [32] K. Zhang, F. Bariani, and P. Meystre, Theory of an optomechanical quantum heat engine, *Phys. Rev. A* **90**, 023819 (2014).
- [33] K. Zhang and W. Zhang, Quantum optomechanical straight-twin engine, *Phys. Rev. A* **95**, 053870 (2017).
- [34] A. Dechant, N. Kiesel, and E. Lutz, All-optical nanomechanical heat engine, *Phys. Rev. Lett.* **114**, 183602 (2015).
- [35] G. Serafini, S. Zippilli, and I. Marzoli, Optomechanical stirling heat engine driven by feedback-controlled light, *Phys. Rev. A* **102**, 053502 (2020).
- [36] M. Bathae and A. R. Bahrapour, Optimal control of the power adiabatic stroke of an optomechanical heat engine, *Phys. Rev. E* **94**, 022141 (2016).
- [37] M. T. Naseem and Ö. E. Müstecaplıoğlu, Quantum heat engine with a quadratically coupled optomechanical system, *J. Opt. Soc. Am. B* **36**, 3000 (2019).
- [38] R. C. Tolman and P. C. Fine, On the irreversible production of entropy, *Rev. Mod. Phys.* **20**, 51 (1948).
- [39] J. P. Sethna, *Statistical Mechanics: Entropy, Order Parameters, and Complexity* (Oxford University Press, New York, 2021), Vol. 14.
- [40] G. T. Landi and M. Paternostro, Irreversible entropy production: From classical to quantum, *Rev. Mod. Phys.* **93**, 035008 (2021).
- [41] M. Brunelli and M. Paternostro, [arXiv:1610.01172](https://arxiv.org/abs/1610.01172).
- [42] J. P. Santos, G. T. Landi, and M. Paternostro, Wigner entropy production rate, *Phys. Rev. Lett.* **118**, 220601 (2017).
- [43] J. P. Santos, L. C. Céleri, F. Brito, G. T. Landi, and M. Paternostro, Spin-phase-space-entropy production, *Phys. Rev. A* **97**, 052123 (2018).
- [44] M. Brunelli, L. Fusco, R. Landig, W. Wiczcerek, J. Hoelscher-Obermaier, G. Landi, F. L. Semião, A. Ferraro, N. Kiesel, T. Donner *et al.*, Experimental determination of irreversible entropy production in out-of-equilibrium mesoscopic quantum systems, *Phys. Rev. Lett.* **121**, 160604 (2018).
- [45] S. Shahidani and M. Rafiee, Irreversible entropy production rate in a parametrically driven-dissipative system: The role of self-correlation between noncommuting observables, *Phys. Rev. A* **105**, 052430 (2022).
- [46] O. Abah, C. O. Edet, N. Ali, B. Teklu, and M. Asjad, Irreversibility in an optical parametric driven optomechanical system, *Annalen der Physik* **536**, 2300400 (2024).
- [47] Y.-P. Wang, G.-Q. Zhang, D. Zhang, X.-Q. Luo, W. Xiong, S.-P. Wang, T.-F. Li, C.-M. Hu, and J. Q. You, Magnon Kerr effect in a strongly coupled cavity-magnon system, *Phys. Rev. B* **94**, 224410 (2016).
- [48] M.-S. Ding, L. Zheng, and C. Li, Ground-state cooling of a magnomechanical resonator induced by magnetic damping, *J. Opt. Soc. Am. B* **37**, 627 (2020).
- [49] Y.-P. Wang, G.-Q. Zhang, D. Zhang, T.-F. Li, C.-M. Hu, and J.-Q. You, Bistability of cavity magnon polaritons, *Phys. Rev. Lett.* **120**, 057202 (2018).
- [50] C. Kittel, On the theory of ferromagnetic resonance absorption, *Phys. Rev.* **73**, 155 (1948).
- [51] C. Gardiner and P. Zoller, *Quantum Noise* (Springer-Verlag, Berlin, 2004).
- [52] E. X. DeJesus and C. Kaufman, Routh-Hurwitz criterion in the examination of eigenvalues of a system of nonlinear ordinary differential equations, *Phys. Rev. A* **35**, 5288 (1987).
- [53] Z.-X. Liu, H. Xiong, and Y. Wu, Magnon blockade in a hybrid ferromagnet-superconductor quantum system, *Phys. Rev. B* **100**, 134421 (2019).
- [54] G. Adesso, D. Girolami, and A. Serafini, Measuring gaussian quantum information and correlations using the Rényi entropy of order 2, *Phys. Rev. Lett.* **109**, 190502 (2012).